Charles University
Faculty of Medicine in Hradec Králové

Anthropometric-biomechanical description of human pelvis based on the principal stiffness and deformation modes

Michal Kuchař

Abstract of the Dissertation

Doctoral Study Programme: Anatomy, Histology and Embryology

Hradec Králové

2022

Dissertation thesis was written during *part-time* doctoral (Ph.D.) study programme Anatomy, Histology and Embryology at the Department of Anatomy, Faculty of Medicine in Hradec Králové, Charles University.

Author: Mgr. Michal Kuchař

Supervisor: doc. MUDr. Dáša Slížová, Ph.D.
Department of Anatomy, Faculty of Medicine in Hradec Králové

Consultant-Supervisor: doc. Ing. Petr Henyš, Ph.D.
Department of Informatics and Interdisciplinary Studies, Faculty of Mechatronics, Technical University in Liberec

Opponents: prof. MUDr. Václav Báča, Ph.D.
Department of Health Care Studies, the College of Polytechnics Jihlava

prof. RNDr. Jaroslav Brůžek, CSc., Ph.D.
Laboratory of 3D Imaging and Analytical Methods, Department of Anthropology and Human Genetics, Faculty of Science, Charles University

This work has been supported by grant SVV 260543/2020.

The dissertation is available for inspection at the Study Department of the Dean´s Office, Faculty of Medicine in Hradec Králové, Charles University, Šimkova 870, 500 03 Hradec Králové (phone 495 816 134).

.....

Name, surname, titles
Chairperson of the Commission for Dissertation Defences
in Doctoral Study Programme *Anatomy, histology and embryology*

Table of contents

Souhrn

Kostra je základní podpůrný systém lidského těla a pasivní složka pro jakýkoliv možný pohyb. Tvar a mechanické vlastnosti kosti jsou dány jak jejím embryologickým původem, tak funkcí. Kost je schopna přenášet mechanické zatížení s optimálním množstvím energie a tento tok energie lze dokumentovat buď mechanickým testováním nebo počítačovým modelováním. Rozhodl jsem se pro druhou z možností a formuloval jsem tuhosti jako jednu z nejdůležitějších vnitřních modalit k určení celkové kvality kostí.

Tuhost jako veličina je široce používaným biomechanickým měřítkem odrážejícím geometrické, topologické a materiálové vlastnosti dané kosti. Je definována jako odpor kosti proti deformaci v reakci na aplikovanou sílu. Cílem disertační práce je studovat a popsat tzv. charakteristickou tuhost kostí pomocí virtuálních modelů založených na snímcích počítačové tomografie a spektrálního rozkladu matice tuhosti. Charakteristická tuhost jako zcela nový deskriptor kostní tkáně bude dále porovnána s lokálním rozložením kostní hustoty i se sadou vybraných antropometrických měření za účelem testování její pohlavní specificity. Pro studium pohlavní rozdílnosti je zároveň nutné vyvinout automatický systém schopný rozpoznat a generovat antropometrické orientační body na kosti.

Lokalizace nejmenších tuhostí a jejich směrů má významný praktický výstup. Vzhledem k tomu, že kvalita kostí přímo ovlivňuje kvalitu života pacienta, jsou nové metody predikce kostní mechaniky velmi zajímavé v různých biomedicínských oborech. Díky této metodice může být v budoucnu možné modelovat riziko zlomenin (boční pády, autonehody), adaptaci skeletu v reakci na specifické zatížení (implantáty) nebo mechanické změny při různých onemocněních (osteoporóza). Vše na základě vyšetření reálných pacientů a neinvazivně.

V této práci se zaměřujeme na nalezení těchto tuhostí a prostřednictvím těchto informací se snažíme lépe porozumět složité anatomii a fyziologii lidské pánevní kosti. Vzhledem k tvarové složitosti i pro úzký funkční vztah k okolním strukturám je nezbytný kombinovaný anatomický a biomechanický přístup.

Summary

Skeleton is a basic supporting system of the human body and a passive substrate for any possible movement, while the shape and mechanical properties of a single bone are given both by the embryological origin and its function. The bone can transfer mechanical load with an optimal amount of energy, and this power flow can be documented by mechanical testing or computational modelling. The author decided on the latter and tried to define the main stiffnesses as one of the most important internal modalities to determine overall bone quality.

Stiffness is a widely used biomechanical measure reflecting geometric, topologic and material properties of a given bone. It is defined as a resistance of a bone against deformation in response to an applied force. This thesis aims to study and describe a characteristic bone stiffness of a CT based virtual models using the spectral decomposition of a stiffness matrix. The characteristic stiffness as a brand-new descriptor of bone tissue will be further correlated with the bone density spatial distribution and matched against a set of chosen anthropometric measurements to test its sex-specificity. Additionally, an automatic system capable of recognising and generating anthropometric landmarks on a bone will be developed as a side result.

The localisation of the smallest stiffnesses and their directions has a significant practical output. As bone quality directly influences patients' lives, novel methods for predicting bone mechanics are of high interest in various medical fields. With proper modelling, one can model the fracture risk (side-falls, car accidents), skeletal adaptation in response to specific loading (implants) or mechanical changes based on different diseases (osteoporosis). Ideally, non-invasively and based on actual patient examinations.

In this thesis, the author focused on finding these stiffnesses to better understand the complex anatomy and physiology of the human pelvic bone. As the bones are different in size and shape, connected to muscles and neighbouring body parts, all these aspects affect bone stiffness's spatial distribution. Here, the combined anatomical and bio-mechanical input is essential.

Background

Introduction

There is a high interest in finding the origin of skeletal fragility, leading to many collaborations between clinicians and anatomists, physicists or engineers. This branching tree of studies of various disciplines clearly shows that there is no simple way to describe bone properties. The complexity of these characteristics led to a proliferation of studies, from nano-structural at the level of collagen structure and mineral crystals to macro-structural describing the whole bone morphology. The methods capable of assessing bone quality components are similarly numerous, from bone resorption biomarkers, chemical analyses, and scanning electron microscopy to X-ray-based imaging modalities.

Although the proportional distribution of previously mentioned characteristics on bone structural behaviour is still discussed, it is possible to quantify their joint influence on whole-bone level through various types of mechanical testing. Each experimental set-up depends on whether the structural strength, toughness or stiffness is to be measured. Being by definition related to fractures, bone strength is a preferable choice in most studies. Recently, one can observe an increased number of stiffness oriented studies as a non-destructive and in-vivo applicable method. Moreover, structural stiffness is probably the main adaptive feature of bone, allowing proper response to incoming loads through the optimisation of bone shape and material. As bone quality directly influences patients' lives, novel methods for predicting bone mechanics are of much interest to clinicians and researchers. A shift from traditional mechanical testing to the digital bone, or 'in silico' models is observed, where elastic properties are derived from computer tomography (CT) scans. However, the necessary cost comes in general simplifying material behaviour to create a practical computational model. The result strongly depends on the quality of input data, which is limited to the macro-structural level at clinical CT. Current machines still don't capture internal bone architectonics properly and often require external calibration to derive bone mineral density (BMD) from attenuation coefficients.

This study tried to predict the bone behaviour according to its characteristic stiffness. In this process, we had to run a number of intermediate steps. Firstly, enough clinical CTs had to be collected, checked for any possible trauma and segmented. Simultaneously, a literature review should be performed to find a suitable density-elasticity relationship (DE-relationship) of bone tissue to fit our biomechanical models. Secondly, we had to quantify the bone morphology as well as density distribution and develop a model of virtual stiffness measurement. The final part was to describe our model's population specificity (spatial, temporal and sex distribution). The organisation of the work is proposed in Fig. 1.

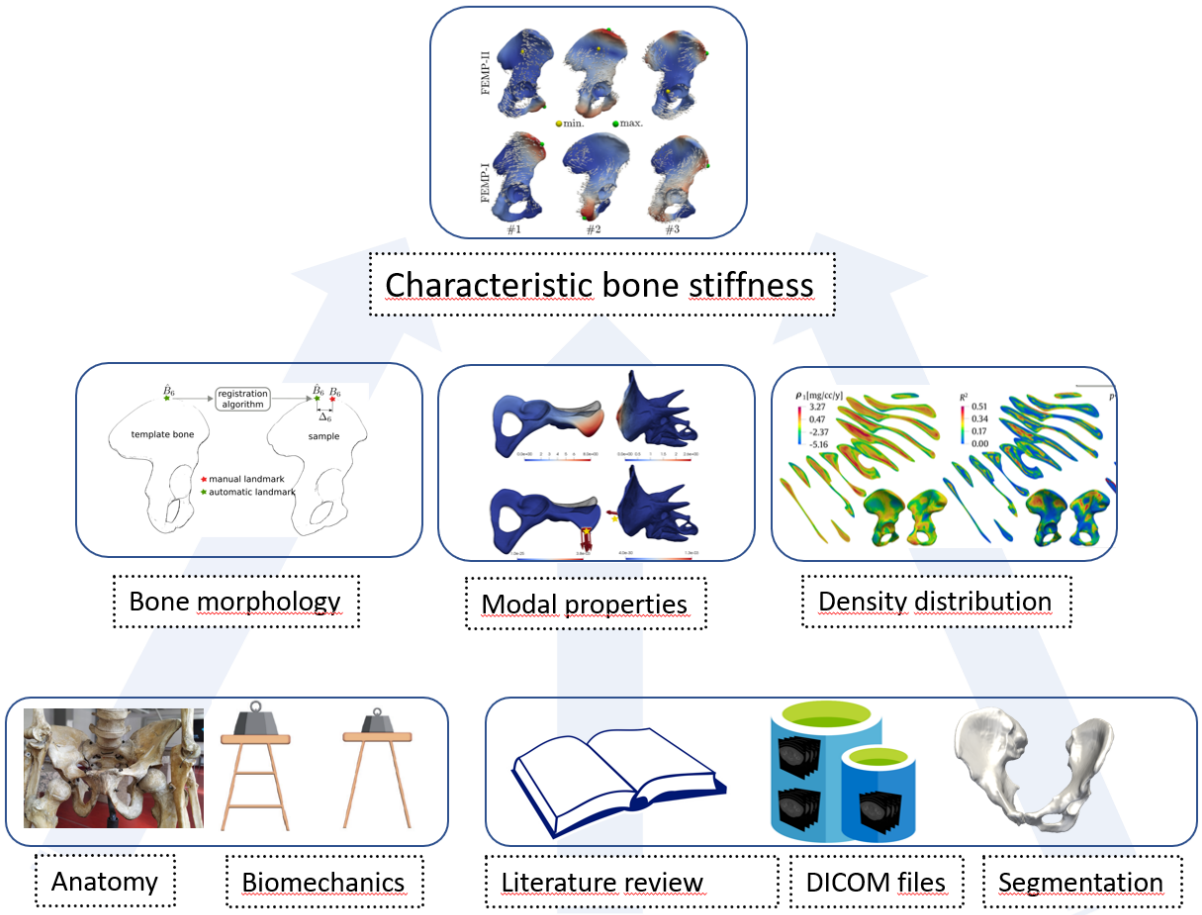

Fig. 1: Study outline. The first step (base of the pyramid) should be an understanding of the bone anatomy and basic biomechanics; to gather and process an appropriate number of patients data; to find a suitable relationship between bone density and elasticity. The second line represents the population-wise definition of bone morphology and density. Further on, the idea of the spectral decomposition of a stiffness matrix is introduced. Finally, the characteristic bone stiffness is derived according to all previous sub-steps and the method implications are discussed.

Literature review of density-elasticity relationship

To map calibrated CT based mechanical properties to FE models, it is essential to apply an appropriate relationship between the bone density and its mechanical properties. In other words, we need to connect the (known) BMD derived from the patient's medical records to (unknown) modulus of elasticity. The newly formed density-elasticity relationship is used to estimate the material stiffness, which will further affect the computations of the structural stiffness.

Setting a study-specific relationship is technically and timely demanding, so we chose the possibility to find the mathematical equations that have been already introduced in the literature. There are many relationships used in clinical/biomechanical papers and for the most accurate modelation, they should be read through and considerably chosen.

Density-elasticity relationship

Two major databases were searched through ScienceDirect and Google Scholar, with search terms "density-elasticity relationships", "finite model of pelvis", "pelvic density", "mechanical analysis of pelvic bone" and "pelvic bone mechanics".

Since the D-E relationship is to be applied to the CT-based data, studies must meet the following criteria:

The human bones are tested exclusively for the human and animal bones significantly differ [1]. The author explicitly describes the relation between the density and Young's modulus; the final equation must be compatible with CT scan data.

There are differences between the mechanical properties of the dry bone, even between the bones of different saturation with fluid. Therefore, the specimen must come from the fresh bone [2, 3].

Most suitable DE-relationship

DE relationship proposed by Keyak et al. [4] seemed most promising to us. The study included specimens with a wide density range, describing the properties of cortical, trabecular and even transition areas. This relation is widely used in related literature therefore, we decided to choose just a slightly modified version capable of improving the results from transition threshold values, as presented and validated in [5-7]:

$$E_{cort} = 10200 \cdot \rho_{ash}^{2.01} \text{ (MPa)}, \quad \rho_{ash} \geq 0.486 \text{ (g/cm}^3\text{)}$$

$$E_{trab} = 2398 \text{ (MPa)}, \quad 0.3 < \rho_{ash} < 0.486 \text{ (g/cm}^3\text{)}$$

$$E_{trab} = 33900 \cdot \rho_{ash}^{2.2} \text{ (MPa)}, \quad \rho_{ash} \leq 0.3 \text{ (g/cm}^3\text{)}$$

Where $E_{cort/trab}$ is the Young's modulus of cortical/trabecular bone and ρ_{ash} is an ash density (ash mass divided by bulk sample volume).

Objectives

The aim of the project is to study and describe a characteristic bone stiffness of a CT based virtual models using the spectral decomposition of a stiffness matrix,

with the following hypotheses:

We can locate the sites of smallest/highest stiffnesses on human pelvic bone.

There is a correlation between these stiffnesses and shape, sex and age.

We can predict the distribution of stiffnesses in the population.

and following implications:

The author will improve his expertise in topics of imaging methods and their processing, creation of finite-element models and their interpretation.

Established big database of pelvic bone models can serve both for this thesis purposes and for consequent studies.

A newly formed shape analysis algorithm will considerably speed up the results acquisition, even allowing later correction of input data. The researcher's experience and practice are here not of importance.

The population-specific bone density and stiffness will improve current biomechanical models. Its outcomes could be further applied in many clinical fields, such as orthopedy, traumatology or endocrinology (osteoporosis).

The characteristic stiffness is potentially a strong inter-individual descriptor and could be used in forensic or anthropological studies.

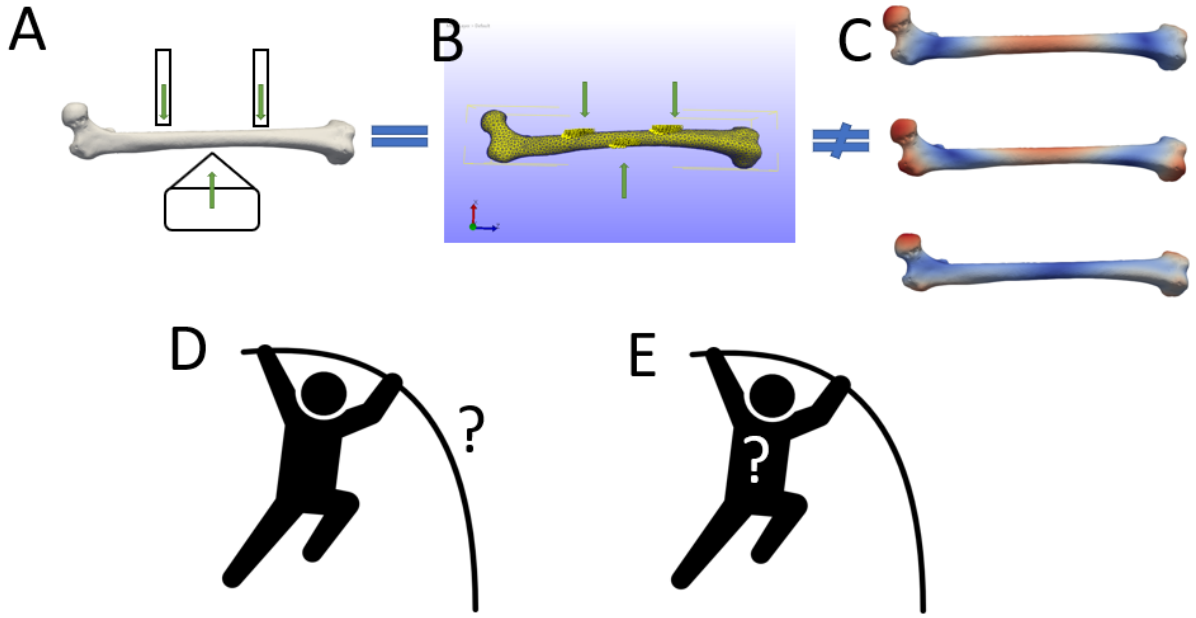

Fig. 2: An explanation of the method novelty. The standard biomechanical 3-point bending test of the long bone (A) can be substituted by FEA simulated virtual measurement, in respect to the original boundary conditions, load magnitude and its direction (B). In our study, characteristic bone stiffness is found independently from the incoming loads, just from known structure morphology and internal structure - even with no boundary conditions defined (C). Both methods describe the structural behaviour with respect to external forces. Traditional approach (D): incoming load is applied to the pole, resulting in its bending. Our approach (E): what type of load should be applied to bend the vault to this typical shape?

Contributions

The dissertation thesis is a part of continuous collaboration between the Faculty of Medicine in Hradec Králové and Technical University in Liberec. We found the synthesis of mathematical and anatomical aspects productive and mutually enriching. The author is the creator of a protocol for collecting CT data from a local hospital database. From this data collection, he segmented pelvic bones, performed anatomical analysis and extracted values of selected tissues for internal calibration of HU units to BMD density.

In the next step, the author proposed the idea of using a registration algorithm to automatically analyse the data in the CT database. He demonstrated the advantages of the registration algorithm in publication [8]. This algorithm became crucial in a further analysis, where the author showed for the first time how bone density changes regionally as a function of age and sex and outlined several original hypotheses that may explain the complex evolution of density in different regions [9]. After analysing BMD density, which is crucial for the determination of bone stiffness, the author came up with the original idea of the existence of a so-called characteristic stiffness that would include both material and structural properties of bone. In collaboration with assoc. prof. Henyš, who provided the technical calculation of the spectral decomposition of the bone stiffness matrix, they found that the smallest bone stiffness could be found without a costly experiment [10]. In the next step, the author analysed the sensitivity of this stiffness to sex and age and demonstrated for the first time that pelvic bone stiffness is strongly sensitive to age and sex and has excellent predictive capabilities for anthropometric analyses [11].

He concluded the paper with an in-depth analysis of the properties of this stiffness, specifically first and second modal stiffness and its associated deformation shapes on a selected sample of femoral bones. In this chapter, he showed that these characteristic deformation modes have the same shape as the deformation under normal movement physiology, thus confirming for the first time that this characteristic stiffness has a deeper meaning and reflects the mechanical design of the bone.

Material and methodology

Original data

The anonymised retrospective CT data were randomly taken from routine examinations in the Faculty Hospital in Hradec Králové under ethical approval 202010P08 and 202102IO2P. The files were stored in DICOM (Digital Imaging and communications in Medicine) format, CT resolution of the dataset was 0.8x0.8x0.8 mm (Siemens Definition AS+, Siemens Definition 128, both Siemens AG, Erlangen, Germany; 120–130 kV using CareDose, reconstruction kernel 80–90, bone algorithm). The inclusion criteria were abdominal CT scans, bones without any trauma, and an age range of 20 years or older. The younger persons were excluded due to unfinished ossification (see Fig.7). The pelvic bone is well suited for our study because of its multifaceted morphology. Moreover, being the most sexually dimorphic skeletal element in the human body, it could further serve as a way of sex identification.

The sample population was equally balanced in sex (100 males, 100 females), with the average age being 64 ± 13.5 years. For bone density evaluation, just 97 females and 88 males were randomly taken from routine examinations in the Faculty Hospital in Hradec Králové. In this case, the sample population age per sex was in the range 22–88 years, divided into ten bins, where each bin contained more than five samples.

One human femur was randomly chosen from the historical osteological collection (property of Anatomy Department, Medical Faculty in Hradec Králové) and CT scanned with the same settings as the clinical CTs. This sample served as a model for method interpretation.

The segmentation process runs in free open-source software MITK-GEM (The Medical Imaging Interaction Toolkit), widely used to generate superficial meshes from bones [12, 13]. The process is presented in Fig. 3. It comprises the image cropping (selection of either left or right pelvic bone), semiautomatic segmentation (to distinguish bone from soft tissues) and finally, surface mesh generation (to allow further use of finite element method).

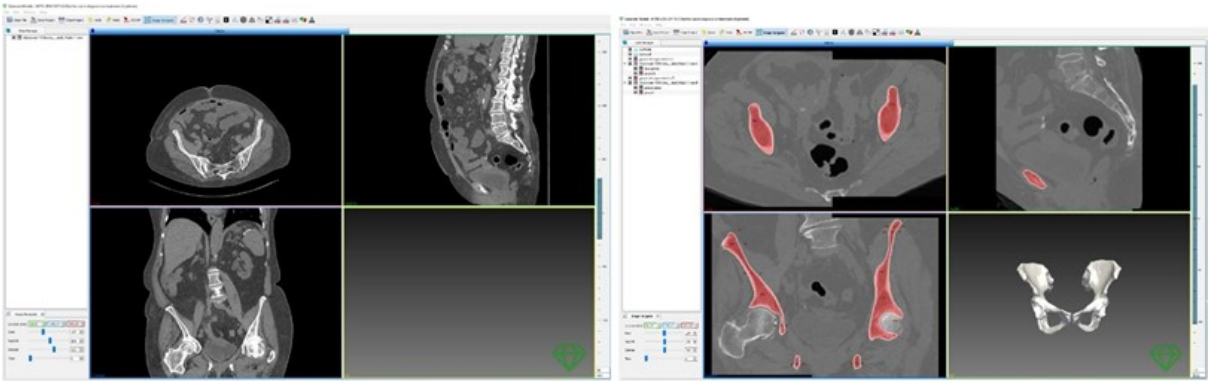

Fig. 3: Process of bone segmentation and surface mask generation.

Shape registration is the following step because each sample (bone) has different sizes and shapes. However, bone samples are anatomically and topologically equivalent. This implies the existence of a point correspondence between two shapes under some suitable class of bijective maps and similarity metrics. To find such a correspondence, rigid and affine transforms were realised for the initial global alignment of bones in dataset, using the ANTs registration library. Then, a non-linear transform was found with the help of the SyN diffeomorphic-based registration algorithm in the ANTs library, see [14]. The similarity of deformed bone shapes was measured with a modified intensity-based criterion called the demons-like metric. The purpose of image registration is to geometrically align the so-called moving image I to the so called fixed image J by a suitable class of maps (Fig. 4). These transformations were computed by a well–known diffeomorphism method SYN in library ANTs with a modified intensity-based criterion called the "demons-like metric". In order to minimise registration error, a template bone shape, which is an estimate of the mean sample shape, was estimated according to [14]. Once the template bone was obtained, all the samples in the dataset were morphed into the template bone shape. Each morphed bone sample was visually inspected for the presence of any errors. Both the original CTs, which hold information about the bone density, and segmented models, describing the bone shape served as a basis for follow-up studies.

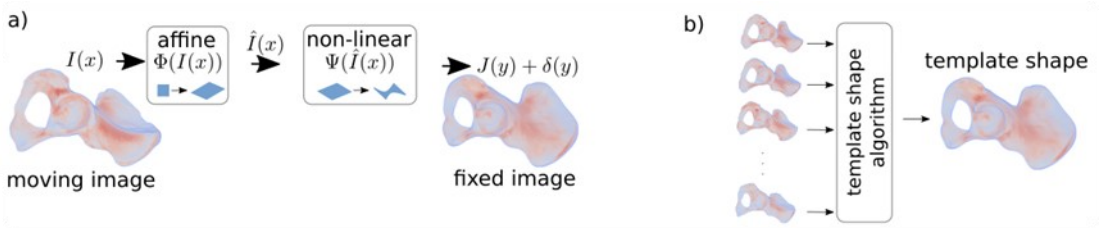

Fig. 4: a) An illustration of the steps of the registration algorithm: the affine transform globally translates, rotates, scales and shears the moving image; the non–linear transform deforms (voxel-wise) the moving image in order to align the moving image with the fixed image. b) The fixed image is a template shape that is estimated from the dataset.

Anthropological Measures

The template bone was set by a group of anthropometric reference landmarks B1, B2, ..., B19 with the associated distances M1, M2, ..., M10 (see Fig. 5), by utilising ParaView software [15]. I adopted the landmarks defined by Murail and Bruzek [16], both for their acceptance in the published literature [17] as well as for their sex–specificity. One additional landmark B20 was added to test the algorithm's accuracy on the concave surfaces (the bottom of the acetabular fossa).

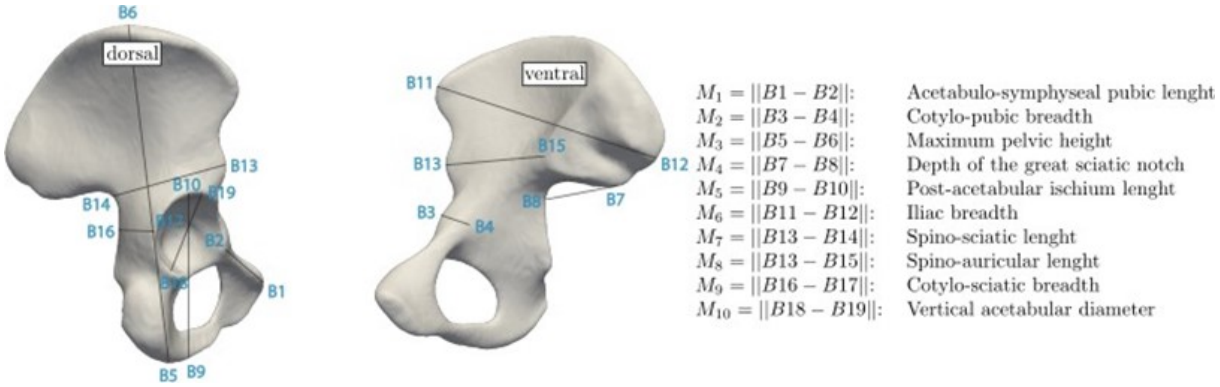

Fig. 5: The estimated shape of the template bone with the reference landmarks B and distances M.

The CT scans were calibrated internally, resulting in BMD [18]. The HU values of air, bone tissue, fat, blood and muscle were considered for internal calibration, as shown in Fig. 6. Only the right-hand side pelvic bone was considered because no significant difference was explored between the left and right sides.

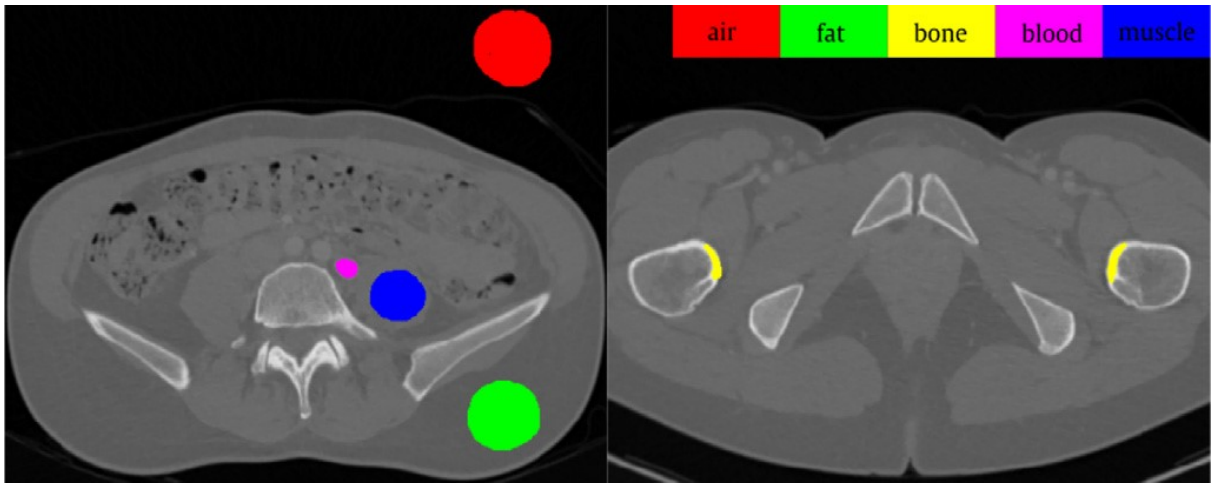

Fig. 6: Example of CT slice where HU values of the considered tissues were selected for internal calibration. ROI content (mm^2): air: 1312; fat: 1109; bone: 160; blood: 92; muscle: 618. Mean HU (standard deviation): air: -1002 (7); fat: -90 (12); bone: 1233 (236); blood: 217 (16); muscle: 60 (12).

CT values were transformed to an effective density in order to compute the total mass of the bones ρeff = bCT, where the scaling coefficient is b = 658 g/cm^3 [19]. The CT scans were calibrated internally to estimate Young's modulus, resulting in hydroxyapatite content in bone [18]. Appropriate density–Young's modulus (see chapter Literature review) was used. The Poisson's ratio ν is defined as a constant 0.3 [19] over the whole bone domain. Two sets of boundary conditions were built. The first model, FEMP-I described the fixed boundary conditions. The fixed boundary conditions were inspired by previous works [20] and mimicked the physiological conditions up to some extent. The second model considers no kinematic and no force boundary conditions, called FEMP-II. Based on the geometry, material and boundary conditions defined, the stiffness and mass matrices K, M are constructed with the help of finite element method.

Results

The Distance Between the Automatically and Manually Seeded Landmarks B

The largest average distance of 15.91 mm was found for landmark B6, while the smallest distance of 2.04 mm was found for landmark B18 in test set 2, see Fig. 7. There were no statistically significant differences between the repetitions of test1 and test2. The lowest value of p was 0.05 for landmark B14, while the highest value of 0.49 was found for landmark B19.

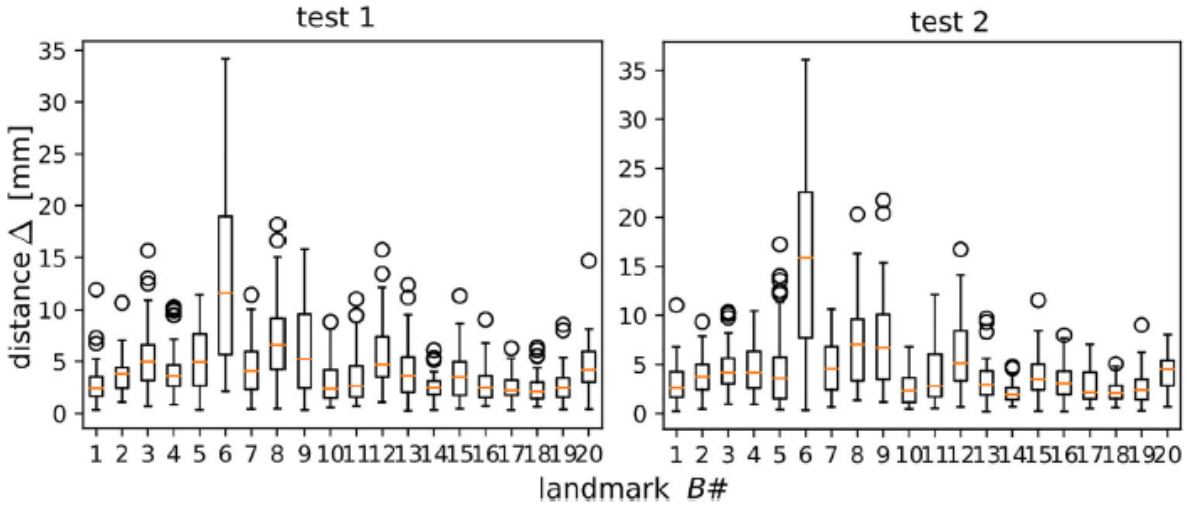

Fig. 7: A boxplot showing the distance between the automatically and manually seeded landmarks for both repetitions.

The Differences Between the Automatically and Manually Computed Distances M

The largest average relative difference of -4.20% was found for distance M4 in test set 2, see Fig. 8. The average lowest relative difference of 0.01% was found for distance M10 in test set 1, see Fig. 8. There were no statistically significant differences between the repetitions of test1 and test2. The lowest value of p was 0.06 for the distance M9, while the highest value of 0.49 was found for distance M2.

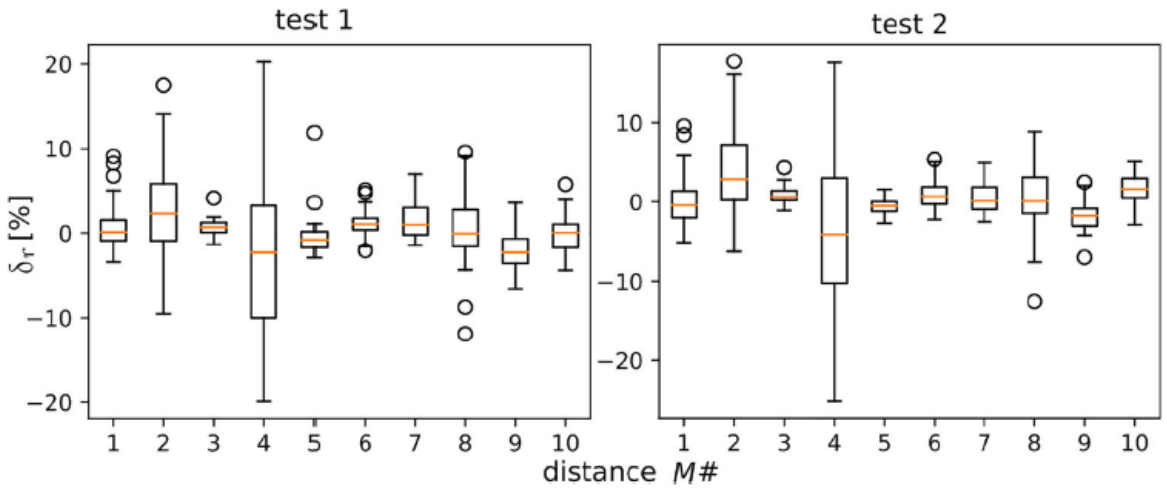

Fig: 8: A boxplot showing the relative difference between automatically and manually seeded landmarks for both repetitions.

Mineral density distribution

The mean and standard deviation functions varied spatially significantly and differed for cortical and trabecular regions and for both females and males, i.e., BMD random fields were non-stationary in space.

Data analysis for females yielded the highest sample mean value of 1.246 (arcuate line, upper third), while the lowest was 0.106 (above the greater sciatic notch). The highest value of sample standard deviation (std) was 0.191 (top of the acetabular margin), while the lowest was 0.015 (deep to the auricular surface

The data analysis for males yields the lowest mean value of 0.119 (deep to the auricular surface), while the highest was 1.135 (uppermost part of arcuate line). The lowest value of std was 0.016 (in between the iliac wing and iliac tuberosity), while the highest was 0.218 (top of the acetabular margin.

Age dependence of BMD/$\overline{\text{BMD}}$

The BMD slope for females varied in range from 5.163 (dorsally to the arcuate line) to 3.269 (above the greater sciatic notch) and from 5.470 (superior-posterior part of acetabular margin)

to 3.625 (anterior third of iliac crest) [mg/cc/year] for females and males. The BMD is intermediately correlated with age (R2 0.51) and (R2 0.49) for females and males, respectively.

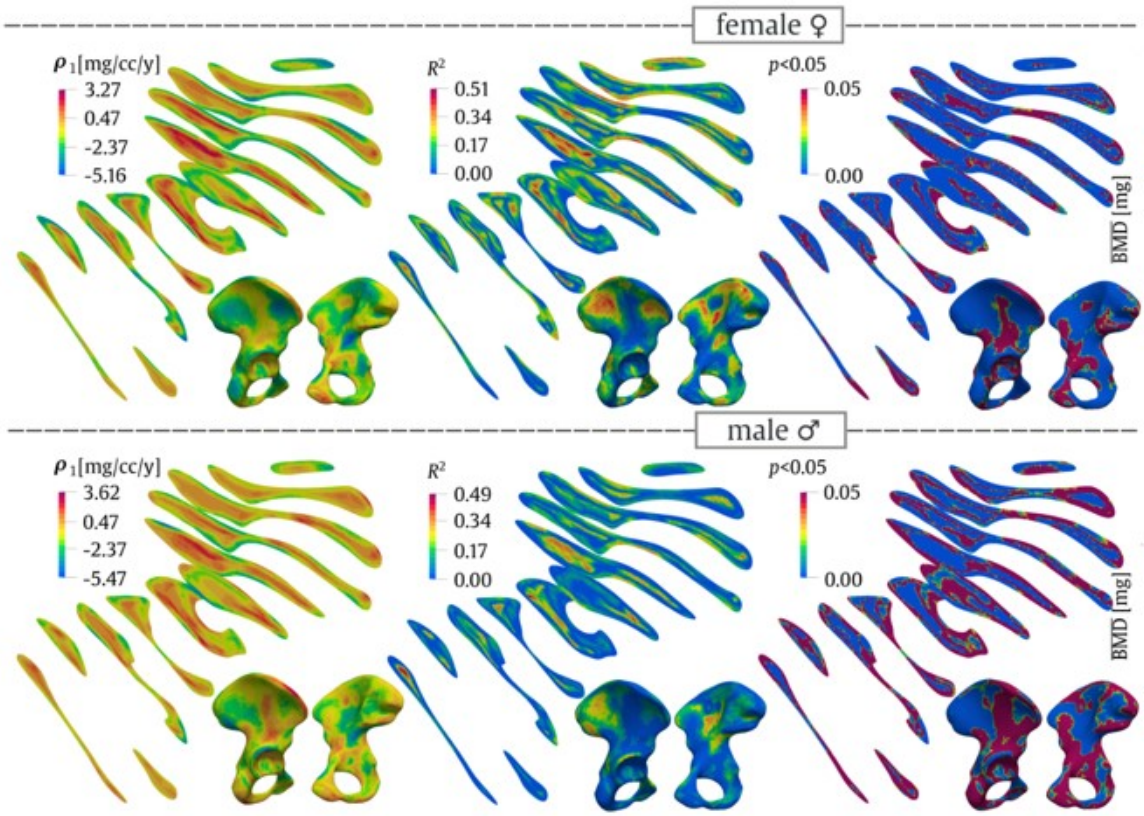

Fig. 9: Spatio-temporal evolution of BMD and $\overline{BMD}$

Characteristic stiffness

Modal Stiffness and Eigenvectors Description

The first eigenvector for model FEMP-I might represent a torsion deformation mode with maximal value located in proximity to the pubic tubercle and minimal value below the termination of the anterior gluteal line, see Fig. 10. The second eigenvector contains two significant deformation zones and is rather of bending character. Its maximum is located at the iliac crest and minimum at the central part of gluteal surface. The third eigenvector is of a rather complex bending deformation, with three localisations at different regions of the iliac wing and

ischiopubic ramus. The minimum and maximum values are localised close to the anterior superior iliac spine and the dorsal portion of the acetabular margin, respectively. The rest higher order eigenvectors quickly become much more complex and there are no significant deformation modes interpretable in terms of bending, torsion nor tension. For model FEMP-II, the maximum value for the first eigenvector is located at the anterior portion of the iliac crest. The maximum value for the second eigenvector is projected to ischial tuberosity and the maximum for the third mode represents anterior superior iliac spine. Minimal values of all foregoing modes are the points of fixation, i.e., the symphyseal and auricular surfaces of the pelvic bone. The smallest static stiffness was found with the first modal stiffness and is different for female and male. For female, the mean static stiffness is 170N/mm with standard deviation 48 N/mm for model FEMP-I and mean 97 N/mm with standard deviation 35 N/mm for model FEMP-II. For male the mean values are 267/206 N/mm with standard deviation 64/59 N/mm for FEMP-I and FEMP-II respective.

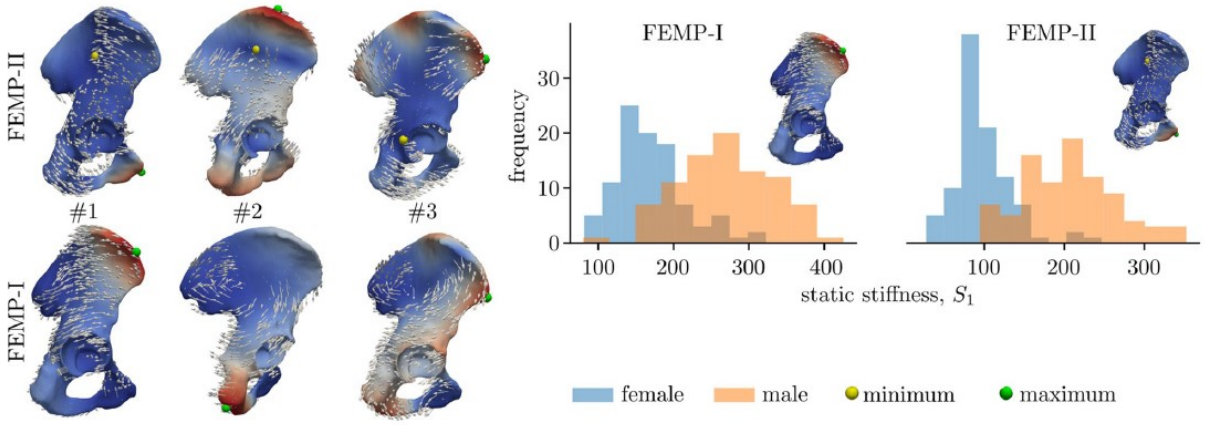

Fig. 10: The description of eigenvectors associated with three modal stiffnesses. The arrows represent the deformation fields. The scalar fields represent the magnitudes of modal vector fields. Minimum markers are not shown for fixed model FEMP-I, given the minima are localised at fixed boundary locations shown in Fig. 5. The histograms show the static stiffness [N/mm], based on the first modal stiffness and considered as the smallest static stiffness.

Comparison of stiffness metrics with anthropometric measures

In case of fixed model FEMP- I, only the first modal stiffness allows to classify sex with an accuracy 85%, while none of modal stiffnesses have the potential to classify the side.

Sex classification accuracy of FEMP-II model is better comparing to FEMP-I. The modal stiffnesses s_1, s_5, s_8 were able to reach a classification accuracy higher than 85%, while none of the modes can classify side. The static stiffness S_1 is also able to predict sex with accuracy higher than 85% according. A highest correlation between modal stiffness and anthropometric distances for model FEMP-II was found in a pair 1-M_2 for male.

Debate

Registration algorithm

According to the results, the automatic measurement method seemed to be accurate and usable for further computation. Most of the average distances between the manually and automatically seeded landmarks were below 5 mm.

The accuracy of automatic landmark seeding depends on the proper seeding of reference landmarks on template bone by an operator. Moreover, the identification of fine anatomical features on template bone can be more difficult because they can be partially smoothed out due to the method used for template bone construction [14]. This situation is typical for landmark B9, which relies on the location of the anteroinferior termination of the ischial tuberosity.

The algorithm calculates a continuous spatial transformation, which means that any point on a bone sample has a unique counterpart on the template bone. In other words, we can potentially define landmarks anywhere on the bone [21]. This transformation makes it possible to interpret the difference in shapes in the deformation metric, which is considered as being intuitive and natural.

Mineral density distribution

Most publications provide information about a gradual reduction in bone mineral density with increasing age [22, 23]. However, it remains unclear whether this is a uniform process for all skeletal sites or whether there might be some region dependence [22-24]. Moreover, due to the variable surface-volume ratio and related bone turnover, local differences between cortical and cancellous bone should be expected [25-27]. The age changes in cortical BMD can be described by cortical thinning, higher porosity, pore diameter and osteon density [28-30]. Cancellous bone is affected by the trabecular loss. In males, this is mostly in the form of trabecular thinning, while in females, trabecular disconnection occurs [31-34]. There is, however, little known about the spatial and age distribution of BMD in human innominate bone, as the majority of studies focus on a long bone, vertebral or hip examinations. Our results showed general age-dependent cortical BMD decline and, surprisingly, local mild trabecular BMD elevation. The reason is unclear, but it could be connected to higher trabecular mineralisation patterns, which correlate

with age, as documented in [35]. We found that female BMD is more sensitive to age. The BMD decreases with age in more than 68%/58% of the volume of bone for females/males. The BMD decreases faster for females (51% faster than for males).

Characteristic stiffness

In this study, ten modal stiffnesses close to zero were presenting 94% of the bone static stiffness. The smallest eigenvalue corresponded to the smallest natural frequency f. Nevertheless, modal stiffnesses do not necessarily follow the same order as natural frequencies since they are rescaled with respect to the power of the eigenvectors amplitude. Interestingly, the modal stiffness corresponding to a first eigenvalue was always the smallest one in our analyses presented here. The corresponding eigenvector maximum magnitude can point to a location and direction of the smallest static stiffness, which can be considered as the most interesting and important. And last, deeper analysis is required to analyse nor explore relations between modal stiffness/smallest static stiffness and important mechanical properties such as bone strength, density and anisotropy.

Stiffness - Sex prediction

Eigen metrics predict sex, although are only weakly correlated with gold-standard anthropometric measures. This fact corresponded to an origin of eigen metrics, which can be seen as spectral components of bone shape information. In fact, the eigen metrics include the topological and intrinsic characteristics of bone apart from geometry information, which cannot be simply captured by the gold-standard method. Further, we include a side classification as a complementary test to validate tested metrics. As was expected, no significant side difference was observed from classification tests with tested metrics. The sex classification accuracy of defined metrics compared to gold-standard seems considerable for individual modes and depends on the boundary conditions defined. Nevertheless, including computed modes simultaneously into the classification algorithm, the final accuracy is excellent (ACC/ACU 98.1%/97.1% 0.01%). Moreover, the sex classification accuracy of gold-standard anthropometric points was also comparably high (ACC/ACU 93.3%/92.1% ± 0.01%).

Boundary Conditions Affect Metrics Sensitivity

We demonstrated that natural frequencies, modal and static stiffness can be computed for a configuration without boundary conditions defined (FEMP-II). This presents a serious advantage, given the proper modelling of often complicated anatomical boundary conditions is difficult and introduces additional uncertainty into the model. Moreover, our results showed that our metrics computed on the model FEMP- II have better description and classification accuracy than a constrained model FEMP-I. In a sex classification, the FEMP-II metrics contain four sensitive eigen pairs, while FEMP-I metrics only one. Moreover, FEMP-II model can be well-validated by an experimental modal analysis with good results [36].

Method interpretation and validation

With the development of the registration algorithm and defying the original bone stiffness metric, the work's intended aim was achieved. However, its full explanation of morphologically and functionally complicated pelvic surpasses the limits of this thesis.

However, our proposed method is transferable to other objects. Once tested on irregular pelvic bones, it could be applied to all bones in a human body, regardless of the complexity/simplicity. I tried to validate the connection between the smallest stiffness modes and physiologically based loads on a bone simpler in geometrical terms – the femur.

Femur – method validation

It is well-known that long bones are the least stiff in pressure, which is reflected in bending mode. However, the direction and magnitude of this deflection depend on the direction and applied force, which is set artificially. The general shape of the femur should counter the main incoming forces with respect to the weight/function ratio. In our opinion, a slightly curved femoral shaft contributes significantly to the material savings, as part of the pressure is transformed into bending. Therefore, stiffness could be a good indicator of bone function. The idea was to simulate the difference in bending modes in the main parts of the gait cycle (stance phase I +II) and compare it with the smallest stiffness distribution acquired by our method. In theory, the modes capable of maximum energy storage (smallest stiffnesses) should correspond to the main loading modes.

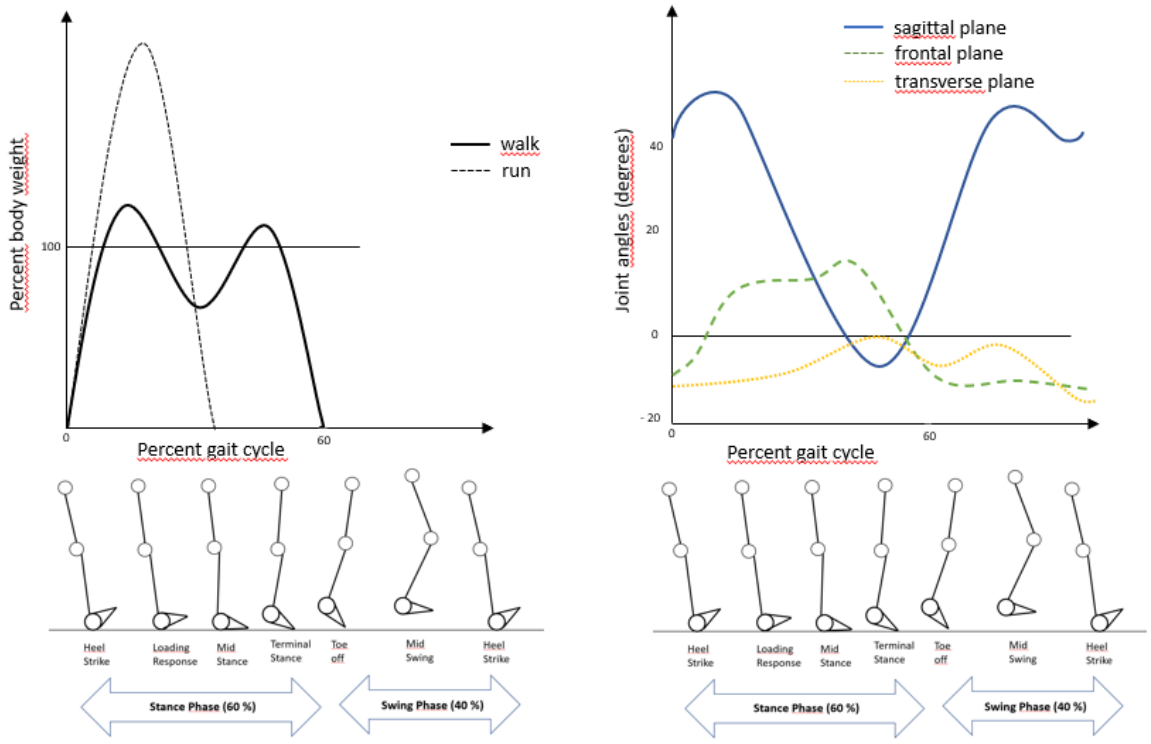

Fig. 11: Distribution of the body weight (A) and hip joint angle value (B) during the separate phases of gait cycle. According to [37].

Preliminary results

For eigenmode1, the main stress distribution is presented on the lateral side of the femoral shaft and medially to linea aspera. We found similar stress distribution in a model of midstance. The stress distribution for eigenmode2 is visually very similar to the model of terminal stance, with the highest values on the medial surface of the femoral shaft and laterally to the linea aspera (Fig. 12).

Both eigenmodes warped by a vector were compared to simulated model deformation in selected gait cycle phases. The results were similar to stress distribution analysis. Eigenmode1 corresponded well to the midstance and eigenmode2 to the terminal stance phase.

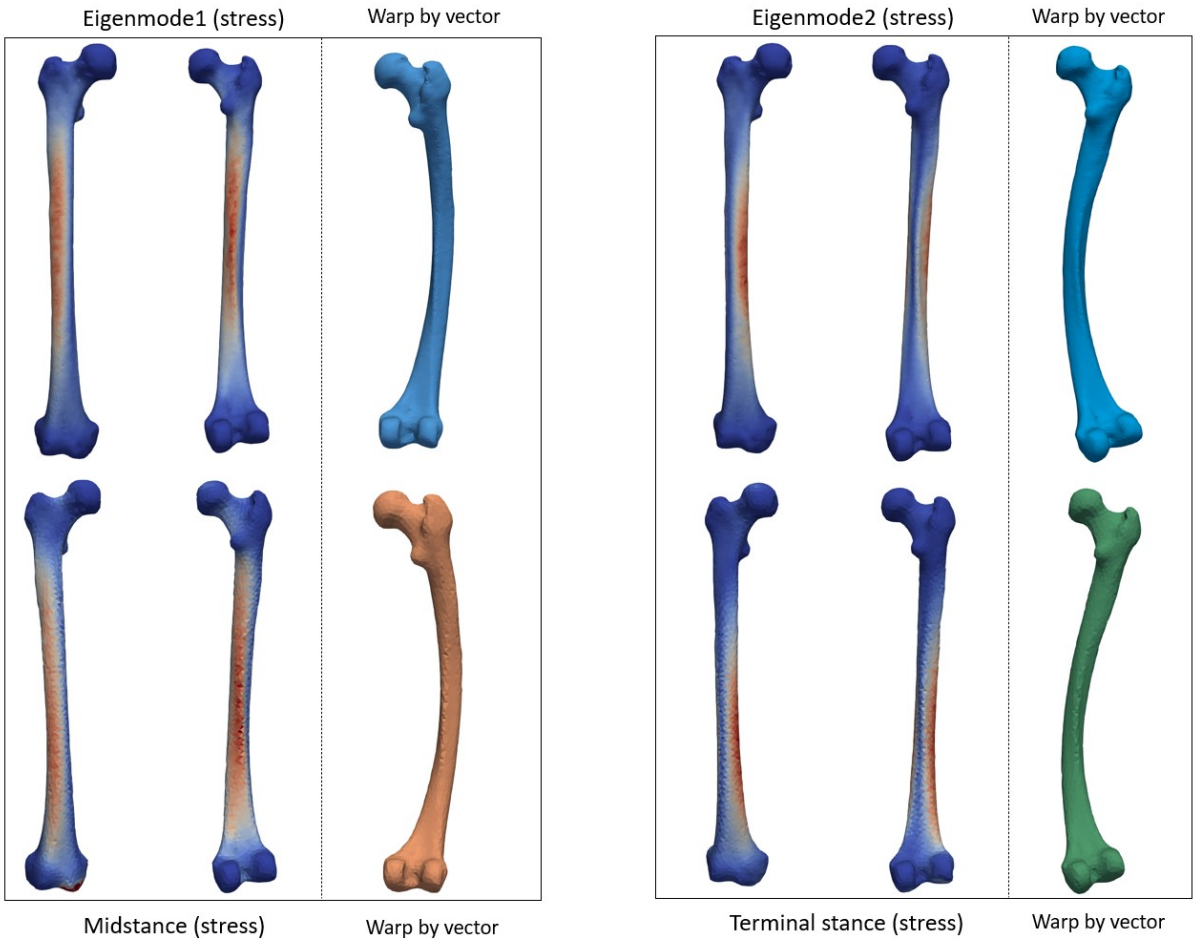

Fig. 12: Stress distribution in eigenmode1 and eigenmode2 with associated deformation modes. The warped models do not represent real bone response under pre-defined load; they visually express displacement amplification according to the vector size and direction.

Contrary to the pelvic bone geometry, the human femur is relatively simple. It behaves like a tubular structure, transferring the body forces towards the ground and works as a lever for muscles of locomotion. As the bone does not change much during human evolution, we assumed that the shape itself (not the internal structure) could be interpreted by the bipedalism requirements, more than resistance to various sudden impacts or individual habitual loading. We compared the outcome of spectral analysis to the behaviour of the bone in two phases of the gait cycle. The results were similar, both for the stress distribution and displacement.

The precise analysis is a topic for further studies. However, here we observed a close connection between stress distribution in the computed eigenmodes and single stance phases of the gait cycle. The spectral analysis results depend purely on geometrical and material properties, not the force direction and value. The ability to "pair "structure's smallest stiffnesses to the

physiological loading could be a promising step in understanding the mechanical behaviour of bones in different anatomical and physiological conditions.

Conclusions

The study utilised the potential of the diffeomorphic shape registration in the automatization of landmark seeding, making data–gathering and its evaluation easier in further process. We created and tested a set of virtual human pelvic bones and defined anatomical landmarks, which were seeded by a proposed registration algorithm. The registration algorithm makes it possible to achieve a high degree of automation with the potential to reduce operator errors in the seeding of anthropological landmarks. This study represents a promising step forward in effectively defining the anthropological measures of the human skeleton and helped us immensely to pair the internal properties of a single bone (stiffness, BMD) with the external properties (bone morphology). The data set of models derived from clinical CT scans was created.

Understanding uncertainties in bone density is of paramount importance to biomechanics in relation to bone mechanobiology, and it should be appropriately incorporated into computational models. We defined the temporal and spatial distribution of the bone mineral density both in the individual pelvic bones as well as population variability. Observed differences indicate that the temporospatial density field is not constant, and further modelling is incomplete without this information.

Structural stiffness plays an important role in bone morphology. The stiffness analysis requires precise experiments and computational models that can be difficult or time–consuming to procure. A new metric for the quantitative and qualitative evaluation of bone stiffness is introduced. It is based on the spectral decomposition of stiffness matrix computed with finite element method, can be easily computed by state-of-the-art subject specified finite element algorithms and provides unique information about the smallest bone stiffness independent from the loading configuration. The metric was compared with anthropometrical measures, tested for sex sensitivity on pelvis bone and interpreted on femoral bone, showing promising results in all cases.

Literature references

1. Currey, J.D., *Tensile yield in compact bone is determined by strain, post-yield behaviour by mineral content.* Journal of biomechanics, 2004. **37**(4): p. 549-556.
2. Martin, R.B. and N.A. Sharkey, *Mechanical effects of postmortem changes, preservation, and allograft bone treatments.* Bone Mechanics Handbook, Second Edition, 2001: p. 20-1-20-24.
3. Cammarata, M., et al. *Mechanical behavior of human bones with different saturation levels*. in *Conference: 2nd International Electronic Conference on Materials*. 2016.
4. Keyak, J., et al., *Validation of an automated method of three-dimensional finite element modelling of bone.* Journal of biomedical engineering, 1993. **15**(6): p. 505-509.
5. Dahan, G., et al., *Finite element analyses for predicting anatomical neck fractures in the proximal humerus.* Clinical Biomechanics, 2019. **68**: p. 114-121.
6. Yosibash, Z., et al., *Predicting the stiffness and strength of human femurs with real metastatic tumors.* Bone, 2014. **69**: p. 180-190.
7. Dahan, G., et al., *Verified and validated finite element analyses of humeri.* Journal of Biomechanics, 2016. **49**(7): p. 1094-1102.
8. Kuchar, M., et al., *Shape morphing technique can accurately predict pelvic bone landmarks.* International Journal of Legal Medicine, 2021. **135**(4): p. 1617-1626.
9. Henyš, P., et al., *Bone mineral density modeling via random field: normality, stationarity, sex and age dependence.* Computer Methods and Programs in Biomedicine, 2021: p. 106353.
10. Henyš, P., et al., *Localising the smallest stiffness and its direction of a homogeneous structure by spectral and optimisation approaches.* Engineering Structures, 2021. **232**: p. 111842.
11. Henyš, P., et al., *Mechanical metric for skeletal biomechanics derived from spectral analysis of stiffness matrix.* Scientific Reports, 2021. **11**.
12. Pauchard, Y., et al., *Interactive graph-cut segmentation for fast creation of finite element models from clinical ct data for hip fracture prediction.* Comput Methods Biomech Biomed Engin, 2016. **19**(16): p. 1693-1703.
13. Helgason, B., et al., *The influence of the modulus–density relationship and the material mapping method on the simulated mechanical response of the proximal femur in side-ways fall loading configuration.* Medical engineering & physics, 2016. **38**(7): p. 679-689.
14. Avants, B.B., et al., *A reproducible evaluation of ANTs similarity metric performance in brain image registration.* Neuroimage, 2011. **54**(3): p. 2033-44.
15. Ahrens, J., B. Geveci, and C. Law, *Paraview: An end-user tool for large data visualization.* The visualization handbook, 2005. **717**(8).
16. Brůžek, J., et al., *Validation and reliability of the sex estimation of the human os coxae using freely available DSP2 software for bioarchaeology and forensic anthropology.* American journal of physical anthropology, 2017. **164**(2): p. 440-449.
17. Quatrehomme, G., et al., *Sex determination using the DSP (probabilistic sex diagnosis) method on the coxal bone: Efficiency of method according to number of available variables.* Forensic science international, 2017. **272**: p. 190-193.
18. Michalski, A.S., et al., *CT-based internal density calibration for opportunistic skeletal assessment using abdominal CT scans.* Medical Engineering & Physics, 2020. **78**: p. 55-63.
19. Taylor, W., et al., *Determination of orthotropic bone elastic constants using FEA and modal analysis.* Journal of biomechanics, 2002. **35**(6): p. 767-773.
20. Watson, P.J., et al., *The effect of boundary constraints on finite element modelling of the human pelvis.* Medical engineering & physics, 2017. **43**: p. 48-57.
21. Málková, M., et al., *An intuitive polygon morphing.* The Visual Computer, 2010. **26**(3): p. 205-215.

22. Demontiero, O., C. Vidal, and G. Duque, *Aging and bone loss: new insights for the clinician.* Therapeutic advances in musculoskeletal disease, 2012. **4**(2): p. 61-76.
23. Khosla, S. and B.L. Riggs, *Pathophysiology of age-related bone loss and osteoporosis.* Endocrinology and Metabolism Clinics, 2005. **34**(4): p. 1015-1030.
24. Riggs, B.L., et al., *Population-based study of age and sex differences in bone volumetric density, size, geometry, and structure at different skeletal sites.* Journal of Bone and Mineral Research, 2004. **19**(12): p. 1945-1954.
25. Ott, S.M., *Cortical or trabecular bone: what's the difference?* American journal of nephrology, 2018. **47**(6): p. 373-376.
26. Wang, X., *Cortical bone mechanics and composition: effects of age and gender*, in *Skeletal Aging and Osteoporosis*. 2012, Springer. p. 53-85.
27. Seeman, E., *Structural basis of growth-related gain and age-related loss of bone strength proceedings of a satellite symposium held on the occasion of the EULAR Congress, Paris, France, June 13, 2008.* Rheumatology, 2008. **47**(suppl_4): p. iv2-iv8.
28. Kranioti, E.F., A. Bonicelli, and J.G. García-Donas, *Bone-mineral density: clinical significance, methods of quantification and forensic applications.* Research and Reports in Forensic Medical Science, 2019(9): p. 9-21.
29. Jepsen, K.J. and N. Andarawis-Puri, *The amount of periosteal apposition required to maintain bone strength during aging depends on adult bone morphology and tissue-modulus degradation rate.* Journal of Bone and Mineral Research, 2012. **27**(9): p. 1916-1926.
30. Nicks, K.M., et al., *Relationship of age to bone microstructure independent of areal bone mineral density.* Journal of Bone and Mineral Research, 2012. **27**(3): p. 637-644.
31. Aaron, J.E., N.B. Makins, and K. Sagreiya, *The Microanatomy of Trabecular Bone Loss in Normal Aging Men and Women.* Clinical Orthopaedics and Related Research, 1987(215): p. 260-271.
32. Ding, M., et al., *Age-related variations in the microstructure of human tibial cancellous bone.* Journal of orthopaedic research, 2002. **20**(3): p. 615-621.
33. Jepsen, K.J., *Functional interactions among morphologic and tissue quality traits define bone quality.* Clinical Orthopaedics and Related Research®, 2011. **469**(8): p. 2150-2159.
34. Chen, H., et al., *Age-related changes in trabecular and cortical bone microstructure.* International journal of endocrinology, 2013. **2013**.
35. Koehne, T., et al., *Trends in trabecular architecture and bone mineral density distribution in 152 individuals aged 30–90 years.* Bone, 2014. **66**: p. 31-38.
36. Henyš, P. and L. Čapek, *Material model of pelvic bone based on modal analysis: a study on the composite bone.* Biomechanics and modeling in mechanobiology, 2017. **16**(1): p. 363-373.
37. Sangeux, M., *Biomechanics of the hip during gait*, in *The Pediatric and Adolescent Hip*. 2019, Springer. p. 53-71.

Overview of own publications:

Original scientific paper(s) published in an impacted journal (with IF)

Kuchař, M., Henyš, P., Rejtar, P., & Hájek, P. (2021). Shape morphing technique can accurately predict pelvic bone landmarks. *International Journal of Legal Medicine*, *135*(4), 1617-1626. **(IF = 2.686)**

Henyš, P., Vořechovský, **M., Kuchař**, M., Heinemann, A., Kopal, J., Ondruschka, B., & Hammer, N. (2021). Bone mineral density modeling via random field: normality, stationarity, sex and age dependence. *Computer Methods and Programs in Biomedicine*, *210*, 106353. **(IF 5.428)**

Henyš, P., Sutula, D., Kopal, J., **Kuchař, M.**, & Čapek, L. (2021). Localising the smallest stiffness and its direction of a homogeneous structure by spectral and optimisation approaches. *Engineering Structures*, *232*, 111842. **(IF 4.471)**

Henyš, P., **Kuchař, M.**, Hájek, P., & Hammer, N. (2021). Mechanical metric for skeletal biomechanics derived from spectral analysis of stiffness matrix. *Scientific Reports*, *11*(1), 1-12. **(IF 4.380)**

Original scientific paper(s) in a journal with editing, but without impact factor

Kuchař, M., Morávek, A., Rejtar P., Henyš, P. (2021). Vliv podkožního tuku, viscerálního tuku a objemu pánevní kosti na obsah kostních minerálů: pilotní studie na rutinních CT. *Clinical Osteology*, 26(4): 200-208.